PHYSICAL REVIEW B VOLUME 44, NUMBER 15 15 OCTOBER 1991-I

InAs quantum dots in a single-crystal GaAs matrix

O. Brandt, L. Tapfer,* and K. Ploog
Max-Planck-Institut für Festkörperforschung, Heisenbergstrasse 1, W-7000 Stuttgart 80, Germany

R. Bierwolf, M. Hohenstein, and F. Phillipp
Max-Planck-Institut für Metallforschung, Heisenbergstrasse 1, W-7000 Stuttgart 80, Germany

H. Lage and A. Heberle
Max-Planck-Institut für Festkörperforschung, Heisenbergstrasse 1, W-7000 Stuttgart 80, Germany

(Received 9 May 1991)

We directly synthesize InAs microclusters embedded in a single-crystal GaAs matrix by molecular-beam epitaxy. Fractional monolayers of InAs are deposited on terraced (001) GaAs surfaces and subsequently overgrown with GaAs. Growth conditions are adjusted *in situ* by reflection high-energy electron diffraction to those favoring step-flow nucleation of both Ga and In adatoms. The resulting microscopic structural configuration is studied by double-crystal x-ray diffractometry and high-resolution electron microscopy. These experiments reveal that InAs growth takes place in fact by nucleation of In adatoms on step edges. An array of isolated InAs clusters of subnanometer size (quantum dots) is thereby formed within the GaAs matrix. The interface of the InAs clusters is in registry with the surrounding GaAs matrix and is thus defect-free. Several spectroscopic techniques, such as transmission, cw photoluminescence, photoluminescence excitation, and picosecond photoluminescence, are applied to get insight into the optical properties of this system. We show that the optical response of excitons attached to the InAs dots is determined by the zero-dimensional symmetry of the system. This effect is most evident when comparing the spontaneous emission of InAs dots and InAs planes, which in either case results from the relaxation of excitons to the emitting state followed by their radiative recombination. The reduced translational symmetry causes a progressive release of wave-vector conservation, thus modifying the selection rules that uniquely determine the interaction of excitons with phonons (relaxation) and photons (recombination).

I. INTRODUCTION

The physics of interacting electrons and holes in spatially confined systems is currently attracting much attention.[1–9] In particular, the interaction of the confined particles with incident radiation is predicted to be strongly modified with respect to that in the bulk crystal.[2–7] Several different attempts have been made to manipulate the dimensions of semiconductor crystals[10] and to control their size in the nanometer regime, with the ultimate aim of reaching the quantum confinement regime where both the translational and relative motion of electrons and holes are frozen out. Two alternative strategies have turned out to be most promising for the realization of semiconductor systems in the nm regime. The first relies on the synthesis of ultrasmall semiconductor microcrystallites, suspended in a dielectric matrix[1,8,9] that serves as the confining potential. This method inherently produces zero-dimensional (0D) systems, but has the drawback that the structural environment is amorphous. Consequently, the surface of a suspended microcrystallite is quasi-free; i.e., it forms by necessity surface states (dangling bonds) that act as centers for nonradiative recombination.[1,8,11] The second approach is the controlled epitaxial deposition of semiconductor multilayers on terraced substrates.[12–14] In principle, this concept offers the possibility to directly fabricated one-dimensional (1D) structures (quantum wires) by the preferential nucleation of adatoms on the step edges. With appropriate growth conditions, this might be achieved even in the presence of a substantial lattice mismatch.[15] However, the inevitable fluctuation of the deposition rates usually results in a poor control of the geometrical configuration and thus the electronic properties of the fabricated structures.[14]

This work (i) reports the direct synthesis of InAs quantum dots by the molecular-beam epitaxial growth of InAs submonolayer films on terraced GaAs substrates and (ii) presents a detailed study of the structural and optical properties of this system. Our approach combines the basic characteristics of the two concepts mentioned above. The controlled deposition of fractional monolayers of InAs on terraced surfaces creates ultrasmall clusterlike units in a confining single-crystal matrix. The arrangement of epitaxial layers in the monolayer regime is dictated solely by the surface morphology, thus relieving us from the requirement of precisely controlling the deposition rates. The well-defined structural environment results in the complete absence of any surface or in-

 ©1991 The American Physical Society

terface states, making this system promising for the study of the intrinsic optical response of ultrasmall 0D systems.

Our work is devoted in equal parts to the understanding of crystal growth, structural configuration, and optical response of InAs clusters in a single-crystal GaAs matrix. Structural information on an atomic scale is provided by high-resolution double-crystal x-ray diffractometry (HRDXD) and high-resolution electron microscopy (HREM). Correlating the results of these techniques, we get detailed insight into the fundamental growth processes on terraced surfaces in the presence of a high lattice strain. Furthermore, these techniques allow us to precisely determine the microscopic structural arrangement of the embedded InAs clusters, which is the indispensable basis for the understanding of the optical properties of this system. Photoluminescence (PL), photoluminescence excitation (PLE), transmission (T), and time-resolved picosecond photoluminescence spectroscopy yield complementary pieces of information on the optical transitions related to the InAs clusters. The optical response of this system is shown to be uniquely controlled by a single parameter, namely, the degree of freedom in translational motion of the exciton attached to the InAs insertions.

The paper is organized as follows. The experimental setup used for our investigations is described in Sec. II. In Sec. III, the preparation of InAs clusters in GaAs epilayers is outlined. Section IV is devoted to the detailed discussion of the structural configuration of these embedded microcrystallites. In Sec. V, we present the results of the spectroscopic investigations. The experimental results are discussed in Sec. VI, putting emphasis on the correlation between structural configuration and optical properties. Finally, in Sec. VII, we summarize the results and draw our conclusions.

II. EXPERIMENTAL SETUP

The samples are synthesized in a three-vacuum-chamber molecular-beam epitaxy (MBE) system, equipped with elemental solid sources providing atomic species of Ga and In and tetrameric As_4 molecules. They are deposited on semi-insulating (001) GaAs substrates, both exactly oriented (No. 1) and misorientated by 3.2° (No. 2) and 6.5° (No. 3) towards [100], respectively. All substrates are mounted side by side on the same molybdenum holder by soldering with In. The growth process is monitored *in situ* by means of reflection high-energy electron diffraction (RHEED), using an electron gun operating at 30 keV under a glancing-angle incidence of 1°.

X-ray diffraction is performed with a high-resolution double-crystal x-ray diffractometer in Bragg geometry. A rotating-anode 12-kW generator with a copper target ($\lambda_{\mathrm{CuK}\alpha 1}=0.154\,0562$ nm) is employed as the x-ray source, and an asymmetrically cut (100) Ge crystal serves as monochromator and collimator. Diffraction patterns are recorded in the vicinity of the (004), (044), (224), and (115) reflections, respectively. The azimuthal orientation of the sample is continuously varied by the computer-controlled rotation around the [001] axis.

For electron microscopy, cross-sectional samples along the [001] direction are prepared by saw-cutting and conventional ion-milling techniques. The specimen thickness is then about 20 nm. Micrographs are taken with a JEM-JEOL 4000FX electron microscope operating at 400 kV with untilted illumination and the objective aperture being centered around the direct beam. Both the {200} and the {220} beams are included in the diffraction aperture and contribute to image formation. Spatial frequencies up to 6 mm^{-1} are transmitted. For image processing, the micrographs are digitized using an EIKONIX camera.

The optical experiments are performed with the samples mounted in an optical flow-through cryostat at 6 K. For photoluminescence, the red line (647.6 nm) of a Kr^+ laser serves as excitation source. Excitation densities from 10 $\mathrm{mW/cm^2}$ to 1 $\mathrm{kW/cm^2}$ are used. The luminescence is focused on the entrance slit of a 1-m single-grating monochromator. A tunable cw dye laser (styryl 9) pumped by an Ar^+ laser is used for photoluminescence excitation, and the excited luminescence is analyzed by a 1-m double-grating monochromator. The excitation density is set to 50 $\mathrm{W/cm^2}$. For the transmission experiments, a broadband 600-W halogen lamp is used as a light source. The intensity of the incident white light is adjusted by means of neutral density filters to 5 $\mu\mathrm{W/cm^2}$. The transmitted light is focused on the entrance slit of a 1-m double-grating monochromator. The emitted or transmitted light is detected in either case by a cooled GaAs photomultiplier operating in the photon counting mode. Time-resolved measurements are performed by pulsed excitation with a synchronously mode-locked Ar^+-laser pumped dye (styryl 9) laser. Excitation intensities of about 500 $\mathrm{nJ/cm^2}$ are used. The emission is dispersed by a 32-cm spectrometer, followed by a Hamamatsu 2D streak camera with a silicon-intensified-target (SIT) Vidicon-readout system and a digital image processor. The overall time resolution of the system is better than 15 ps, including dispersion of the spectrometer.

III. SAMPLE PREPARATION

The crucial point in our method of sample preparation is the existence of a well-defined step structure on the growth surface. To preserve the step structure present on the vicinal substrate throughout the epitaxial deposition, GaAs has to nucleate by step propagation. The growth conditions of the GaAs matrix are thus carefully adjusted to favor nucleation at step edges. The essential parameters are the effective temperature and the beam fluxes arriving on the surface, which determine the adatom diffusion as well as the incorporation kinetics. Both the effective temperature and the net fluxes on the surface are calibrated *in situ* by RHEED. The arriving Ga flux (depositon rate) is set by means of RHEED-intensity oscillations to 1 (ML)/s. 1 ML GaAs refers to the complete coverage of the (001) surface with Ga, corresponding to 6.24×10^{14} cm^{-2}Ga atoms. The As_4/Ga flux ratio is calibrated by arsenic-induced RHEED oscillations to the lowest possible value, just establishing the As-stabilized (2×4) reconstruction during growth. The temperatures

mentioned in the present work are referred to the evaporation of the native oxide at 580 °C and to the transition from the As-stabilized to the Ga-stabilized regime at around 630 °C, as observed by monitoring the RHEED pattern during the substrate preparation. On the vicinal substrates, RHEED oscillations are hardly observed for temperatures higher than 570 °C, indicating that growth above this temperature proceeds entirely by step propagation.[16] However, the temperature must be chosen not higher than a critical value, above which the terrace configuration undergoes a morphological instability.[17] Hence, we set the temperature for GaAs growth to 580 °C.

Prior to the deposition of the InAs/GaAs heterostructure, a 2-μm GaAs buffer is grown at 580 °C in order to improve the homogeneity of the terrace size distribution.[18] During the growth of the buffer, we observe the characteristic splitting of the reconstruction streaks with the electron beam parallel as well as perpendicular to the steps, which reflects the existence of an island structure on the surface.[19] Furthermore, the satellite streaks are found to sharpen during the deposition, corresponding to an increasingly homogeneous island-size distribution.[20]

To initiate InAs deposition, the temperature is lowered to 420 °C. The In shutter is then opened two times for the growth of 0.8-ML InAs, each followed by 2-min growth interruption. The choice of the growth temperature, which is, in fact the one used also for InAs growth on singular surfaces, is motivated by the evolution of satellite streaks during InAs deposition at different temperatures. The satellite streaks are still well resolved after the deposition of InAs at the growth temperature of 420 °C. However, the splitting of the streaks disappears for a lower growth temperature ($\simeq$380 °C) and transforms into V-shaped diffraction features. This shows that for sufficiently high temperatures (420 °C), InAs growth occurs mainly by step-edge nucleation, thus preserving the step structure on the surface. In contrast, the terrace configuration on the surface is unstable due to terrace nucleation and subsequent islanding if the temperature is too low (380 °C) to allow In adatoms to reach the favored nucleation site, namely, the step edge. Finally, before heating up to the growth temperature of the GaAs matrix (580 °C), 3 ML of GaAs are deposited on top of the InAs film at 420 °C in order to avoid the desorption of the deposited In.

IV. STRUCTURAL ANALYSIS

A. Double-crystal x-ray diffractometry

In Fig. 1 we show the experimental (dotted line) and theoretical (solid line) x-ray diffraction pattern in the vicinity of the (004) reflection for the reference sample (No. 1) (a) and sample No. 2 (b), misoriented by 3.2° towards [100], respectively. The theoretical diffraction pattern superimposed onto the experimental one is calculated within the framework of the dynamical diffraction theory, allowing us the accurate determination of the layer thickness (i.e., In coverage) and the strain distribution, as summarized in Table I. Diffraction around symmetric reflections [(044), (244), (115)] demonstrates that the InAs unit cell is in registry with the GaAs lattice; i.e., the lattice mismatch of 7.16% is entirely accommodated by an elastic biaxial compression in the (001) plane, resulting in the tetragonal distortion of the In—As bonds in the [001] direction. The observation of Pendellösung fringes in the vicinity of the main epitaxial reflection (Fig. 1) demonstrate that both heterostructures are of excellent crystal quality. The deviation from the calculated pattern in this region originates from inevitable diffuse scattering at point defects in the substrate, which is more evident for sample No. 2 owing to the lower In content. The important result extracted from the experiments shown in Fig. 1 is that the average In coverage in these two samples is drastically different, namely, 0.8 ML for sample No. 1 and 0.3 ML for sample No. 2. The In corporation is apparently considerably lower in the presence of steps on the surface, evidencing the change in growth mode. If nucleation proceeds by step propagation, adatoms attaching the step edge experience the high strain existing at the edge both parallel *and* normal to the plane. This strain obviously acts as a large kinetic barrier for the final incorporation,[21] resulting in an effective sticking coefficient far below unity. During the overgrowth with GaAs, the excess In segregates to the surface and is desorbed when heating up to the growth temperature of the matrix.[22] Our finding is thus consistent with a step-edge nucleation process of In adatoms.

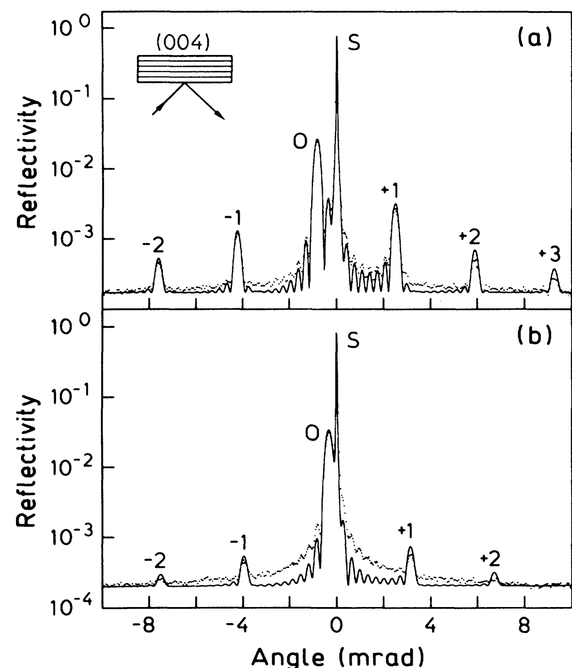

FIG. 1. Experimental (dotted line) and simulated (solid line) x-ray-diffraction patterns in the vicinity of the symmetric (004) reflection for the reference sample (a) and sample No. 2 (b). The deviation of experiment and theory in the vicinity of the main epitaxial reflection comes from diffuse scattering at point defects within the substrate.

TABLE I. Structural parameters of the InAs/GaAs heterostructures of this work. Listed are the average In coverage δ, the separation of the InAs planes D, the lattice strain perpendicular ($\varepsilon_\perp$) and parallel ($\varepsilon_\parallel$) to the plane with respect to the InAs lattice constant (all determined from calculated x-ray-diffraction patterns fitted to the experimental ones), the angle of misorientation ϕ and the mean terrace size L (representing the geometrical average as given by the misorientation angle).

Sample no.	δ (ML)	D (ML)	$\varepsilon_\perp$	$\varepsilon_\parallel$	ϕ	L (nm)
1	0.8	97	0.0726	−0.0668	≤0.1	
2	0.3	97	0.0726	−0.0668	3.2	7
3	0.3	97	0.0726	−0.0668	6.4	3.5

The presence of the terraced surface should manifest itself in an angular shift of the satellite reflections for different azimuthal orientation of the sample.[23] In fact, an asymmetry of the angular position of the satellite peaks (±1) is observed when rotating the crystal around the surface normal. This finding proves the existence of InAs regions that are tilted with respect to the (001) lattice planes of the GaAs matrix.

B. Transmission electron microscopy

For a detailed insight into the structural arrangement of these InAs regions, high-resolution electron microscopy is employed. For the preparation of cross-sectional specimen, the actual surface morphology has to be considered. Figure 2 depicts an illustrative sketch of the situation we are dealing with. The figure shows schematically InAs aggregates formed at the step edges, provided by the specific terrace configuration that is induced by the surface tilt towards [100]. As the experimental micrograph is formed by projection of the whole specimen thickness (≃20 nm), the surface must not have steps in the direction of projection. Steps running along this direction form a staircase whose projection would appear as a band in the micrograph. Cross-sectional samples must therefore be cut along the [100] direction and viewed along the [010] direction, as indicated by the three beams intersecting the specimen. From an intuitive point of view, the step configuration is then expected to be visible in projection; i.e., both height and distance of steps occurring at the surface may then be measured. In addition, if isolated clusters were formed on the terrace edges, a distinct contrast modulation is expected to be observed as a consequence of the different amount of InAs intersected by the beam. As will be shown below, this intuitive argument holds also for the rigorous quantitative treatment of the problem. The observation of this characteristic contrast modulation can thus be taken as the manifestation of the existence of isolated InAs aggregates formed at the terraces. For further statements, however, one has to consider that the terrace configuration shown in Fig. 2 represents a highly idealized case. In reality, steps may meander in both lateral and vertical directions, and aggregates formed on the terraces are superimposed in projection. Moreover, any deviation from regularity of the cluster shape will additionally complicate the image formation, preventing, e.g., the quantitative evaluation of the cluster shape and size.

In Fig. 3(a), the experimental high-resolution lattice image of sample No. 3, misoriented by 6.4° towards [100], is shown. Dark regions appear periodically along the [100] direction, tilted with respect to the (001) planes by 6.34°. Besides the change in contrast, these regions exhibit a spatial frequency which is double that of the surrounding GaAs matrix. For a reliable interpretation of these observations, we (i) process the micrograph by an algorithm that enhances the contrast between the dark regions and the surrounding matrix [Fig. 3(b)], and (ii) perform extensive image simulations for a range of defocus values and specimen thicknesses [Fig. 3(c)]. The contrast-enhancing algorithm exploits the characteristic variations in both contrast and spatial frequency occurring in the experimental image. The simulated images are computed assuming the presence of InAs and regions inside a GaAs matrix. These regions are assumed to be 2 ML thick and to extend either 10 or 20 nm in the direction of projection. The simulations depicted in Fig. 3(c) together with an enlarged portion of the corresponding micrograph clearly demonstrates that the contrast formation is directly determined by the amount of In present in

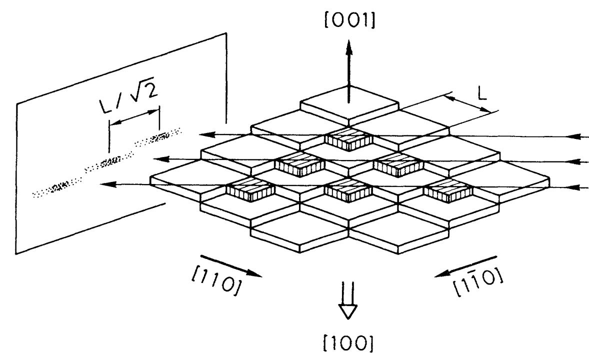

FIG. 2. Sketch of InAs clusters (shaded boxes) grown at the step edges of the terraces formed on the vicinal (001) GaAs surface tilted towards [100]. The specific terrace configuration of this surface consists of two adjacent staircases with steps running along the [110] and [1$\bar{1}$0] directions. The long arrows intersecting the clusters represent the electron beam of the transmission electron microscope. On the left, the resulting projection of the clusters along the [010] direction is depicted. The period of their occurrence is determined by the terrace size L as well as the geometrical arrangement of the clusters on the terraces. The terrace size L is determined by the degree of misorientation $L = a/(\sqrt{2}\tan\phi)$, where a is the lattice constant and ϕ is the misorientation angle as listed in Table I.

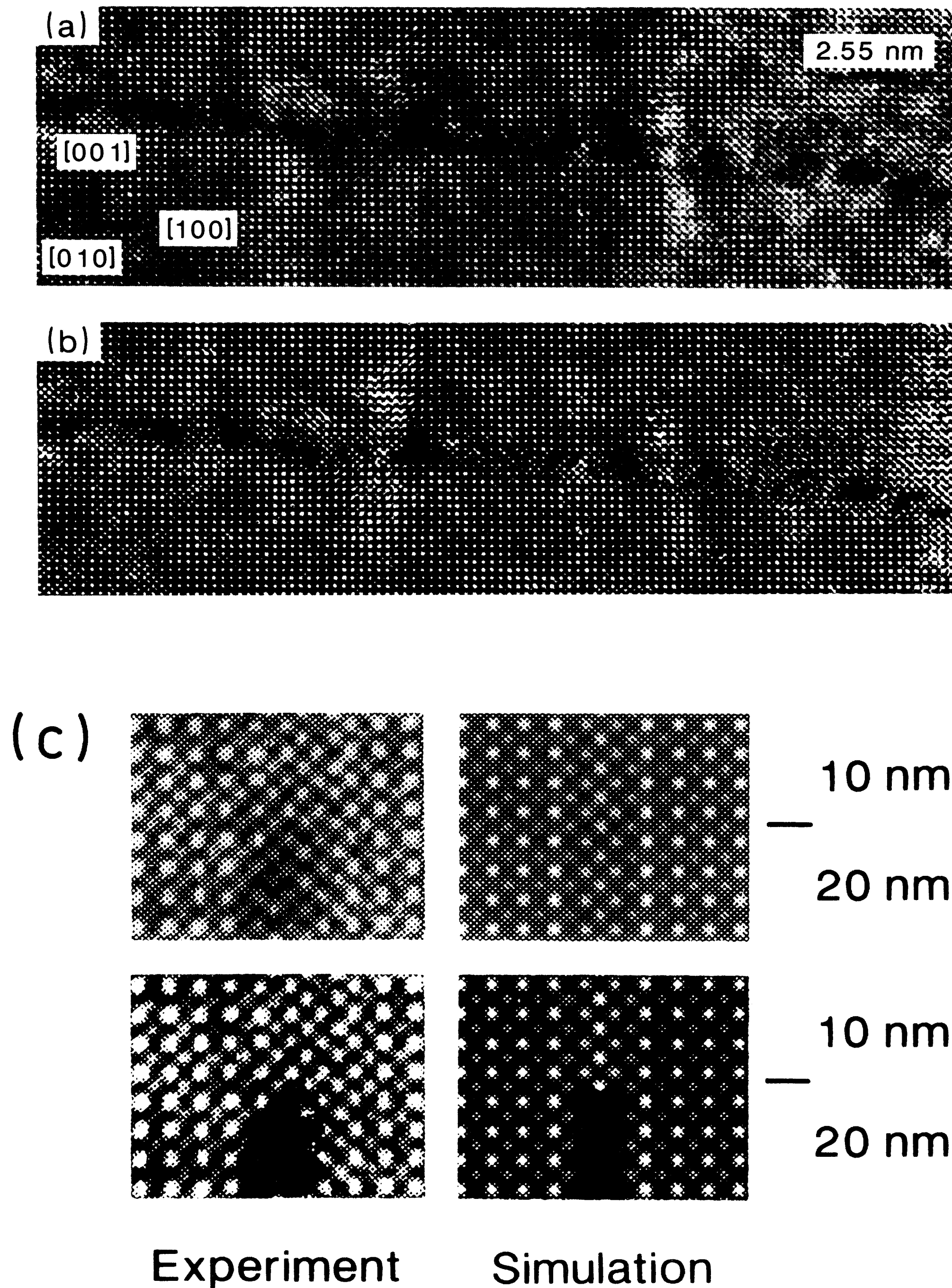

FIG. 3. High-resolution lattice image of sample No. 3. The micrograph is taken along the [010] direction. In (a), the experimental image is shown, Overlapping areas of the sample are connected to examine the spatial distribution of the inserted InAs. The whole probe area is 10×30 nm^2. In (b) the reconstructed image after processing with a contrast enhancing algorithm is presented. In (c), we show on the left side an enlarged portion of the original (upper trace) and the processed (lower trace) experimental micrograph, and on the right side the corresponding image simulation. In the image simulation, the 20-nm-thick cross section is assumed to consist either of 100% or 50% In along the direction of projection, as denoted in the figure. The presence of InAs manifests itself in contrast to the surrounding GaAs (20 nm) as well as in the double spatial frequency (10 nm). Thus the observations of both an unchanged contrast and spatial frequency reveals the absence of InAs. In the experimental lattice image [(a),(b)], InAs clusters appear with a period of 2.5 nm, corresponding to the terrace size of the surface. The cluster location is tilted with respect to the (001) plane by 6.34°, in agreement with the nominal misorientation angle of the substrate. The interface between each cluster and the surrounding matrix is coherent; i.e., no defects are detected in the whole probe area. The contrast variation visible in this picture reflects an upper limit of the cluster size.

the direction of projection, as expected intuitively. However, the presence of In manifests itself additionally by the double spatial frequency with respect to the surrounding GaAs matrix. This phenomenon originates from the different phase shifts for GaAs and InAs. For the selected defocus value, the lattice image is formed solely by the {200} beam in the case of GaAs, whereas both {200} and {220} beams contribute to the image formation for InAs.

With this knowledge, it is straightforward to interpret the original [Fig. 3(a)] and processed [Fig. 3(b)] lattice image. The black regions appearing in the image correspond to regions containing predominantly InAs throughout the specimen thickness. Note that the spatial extent of these black regions is systematically larger than the actual physical size of the InAs location. Between the dark regions, the lattice of GaAs is observed to continue. Thus, the InAs clusters are separated from each other along the [100] direction. Regions where no contrast variation occurs but the spatial frequency changes contain less InAs along the direction of projection. In particular, this conclusion applies to the case of the missing dark region in the center of the image, where InAs is still present in the [010] direction.

Two important facts are demonstrated by the lattice images in Fig. 3. First, the image reveals that isolated InAs clusters are formed within the GaAs matrix. The high periodicity of their occurrence is an indication for the step-edge nucleation of In adatoms. The period apparent from the lattice image is typically 4–5 lattice constants (2.27–2.83 nm), in agreement with the mean terrace size given by the actual tilt angle of 6.34° (see Fig. 3). Biatomic steps are thus homogeneously distributed along the tilt direction. Second, the internal interfaces between InAs and GaAs are free from defects [see Fig. 3(a)], which is not obvious considering the high strain between the two materials.

Note that the precise quantitative determination of the actual cluster size is prevented by the inherently existing fluctuation of the terrace configuration, as already mentioned above. However, image simulations have shown that the observed cluster size in either case represents an *upper* limit for the actual one. The actual dimension in both the vertical and lateral directions is indeed in the subnanometer range.

V. SPECTROSCOPIC INVESTIGATION

In Fig. 4 we show the photoluminescence spectra under cw excitation of the samples under consideration. A single emission band located at around 1.465 dominates the spectra in each case. The integrated intensity of these bands exhibits a strictly linear dependence on excitation density in the range from 10 mW/cm^2 to 1 kW/cm^2, which shows that a purely radiative decay channel is introduced by the InAs insertions. The emission bands of the samples No. 2 and 3 on vicinal substrates are systematically shifted to higher energies with increasing misorientation, accompanied by a strongly asymmetric broadening to higher energies. Neither the spectral position nor the line shape of each of the bands depends on

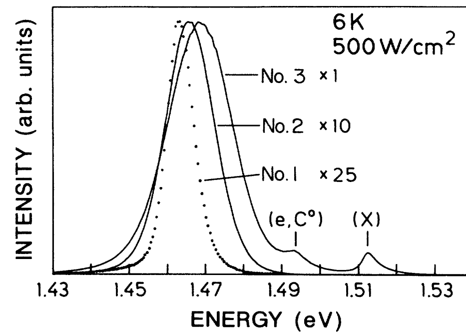

FIG. 4. CW photoluminescence spectra obtained at 6 K of sample No. 1 (dotted line), No. 2, and No. 3 (solid lines). The low-energy transition originates from the radiative decay of excitons attached to the InAs planes (dotted line) and InAs quantum dots (solid lines). The high-energy bands labeled (X) and (e,C^0) stem from the radiative decay of free excitons and the free-to-carbon transition in the GaAs matrix. The peaks are normalized to each other by multiplying them with the factors denoted.

excitation density. On the low-energy side of the bands, an exponential tail occurs for the samples on vicinal substrates. The formation of InAs monolayers having additional atomic steps on top results in a strong red-shift (about 30 meV) of the emission band.[24] This phenomenon is actually observed on samples grown at lower temperatures (380 °C). The absence of any low-energy broadening thus reveals the absence of island nucleation and confirms that growth proceeds indeed by step propagation. In addition, the spectra shown in Fig. 4 reveal a systematic increase of the luminescence efficiency with decreasing terrace size. This striking finding demonstrates that states acting as nonradiative recombination centers are not created at the internal interfaces, in contrast to the case of microcrystallites embedded in an amorphous matrix.[1,8,11] Finally, by collecting the excited emission normal to the {110} cleavage edge (the edge emission mode) instead of normal to the (001) surface (the surface emission mode), its polarization with respect to the InAs plane is measured. The emission of sample No. 1 is found to be polarized parallel to the plane, whereas that of samples No. 2 and 3 is unpolarized. This finding indicates that the electronic state created by an InAs plane and an InAs dot have different symmetries with respect to the plane; namely, anisotropic symmetry for the InAs planes and isotropic symmetry for InAs dots.

To clarify the different emission characteristics obtained from the reference sample No. 1 on the singular surface and the samples on terraced surfaces (Nos. 2 and 3), we compare PL, PLE, and T spectra of samples No. 1 and 3 in Fig. 5. The essential parameters deduced from these and the time-resolved measurements discussed in the next paragraph are summarized in Table II. In each of the spectra, a single transition is seen that corresponds to the one observed in the corresponding PL spectrum (Fig. 4 and the lower trace of Fig. 5). The appearance of

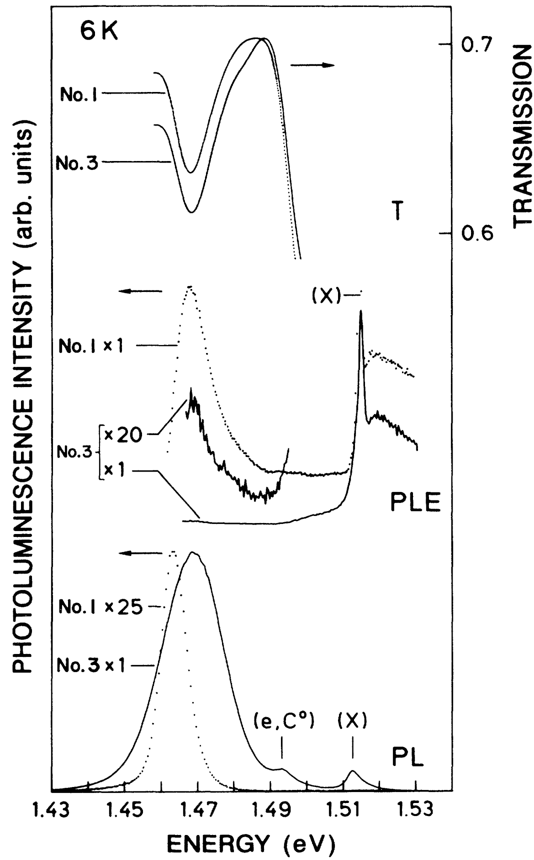

FIG. 5. Photoluminescence (PL), photoluminescence excitation (PLE), and transmission (T) spectra taken at 6 K from sample No. 1 (dotted lines) and sample No. 3 (solid lines). The spectra are multiplied by factors as indicated. The peaks are labeled according to Fig. 4.

distinct resonances in PLE and T reveals the excitonic nature of the transitions. For sample No. 1 the resonances in the PLE and T spectra are Stokes shifted with respect to the PL peak energy to about 5.5 meV. In contrast, for sample No. 3 no Stokes shift occurs between the resonance in the T and PLE spectra with respect to the emission peak in its PL spectrum. Actually, the energy position of the transitions on PLE and T spectra are nearly equal for samples No. 2 and 3 (see Table II). The blue shift of the emission band thus results from the absence of Stokes shift in sample No. 3. Simultaneously, the high-energy broadening of the PL band of sample No. 3 is not observed in its PLE and T spectra. The broadening therefore does not originate from an inhomogeneously broadened density of states, which we might suspect to be caused by a distribution of InAs dot sizes. On the contrary, as revealed by the coincidence of the transition energies for InAs planes and dots, the *energy* of the respective state does not depend on the extent of the InAs cluster, as will be discussed below.

However, the *strengths* of the respective transitions are drastically different for the two samples. The luminescence efficiency under nonresonant excitation is much higher for sample No. 3 than for sample No. 1, as already mentioned above. The opposite is true when examining the luminescence efficiency in quasiresonant conditions, as is evident by comparing the PLE peaks in Fig. 5. The resonance observed in the T spectra in turn is stronger for sample No. 3; i.e., the PLE spectrum is not simply proportional to the absorption probability as seen in transmission.

To get insight into the recombination dynamics in these structures, the temporal evolution of the emission is monitored by picosecond photoluminescence (Fig. 6). The emission of sample No. 1 [Fig. 6(a)] is characterized by a slow rise ($\simeq 85$ ps) and a rapid decay of the luminescence intensity. In contrast, the emission intensity of sample No. 3 rises quickly ($\simeq 30$ ps) and exhibits a much slower decay. The spectrally integrated emission exhibits an exponential decay for both samples, consistent with the expected monomolecular decay of excitons. Since the exciton decay is purely radiative at this temperature, as demonstrated by the linear dependence of the luminescence efficiency on excitation density, the observed decay time of the luminescence is identical to its radiative lifetime. The lifetimes are determined by fitting the luminescence decay with a single exponential to be 115 ps for sample No. 1 and 660 ps for sample No. 3. Finally, the emission bands spectrally diffuse in the course of time in opposite directions, namely, 2 meV to the red for sample No. 1, and 2 meV to the blue for sample No. 3.

TABLE II. Optical parameters of the InAs/GaAs heterostructures of this work. Listed are the spectral position E of the InAs-related transition in transmission and photoluminescence-excitation spectra (Fig. 5), the oscillator strength per unit mesh $\tilde{f}$ determined from the transmission resonance (Fig. 5), the Stokes shift Δ between E and the spectral position of the corresponding band in photoluminescence spectra (Fig. 5), the spectral diffusion Δ_t and the rise time t of the emission observed in transient photoluminescence spectra (Fig. 6), and the radiative lifetime τ_r of the excitons determined by the decay of the spectrally integrated emission (Fig. 6).

Sample no.	E (MeV)	$\tilde{f}$ (10^{-2})	Δ (meV)	Δ_t (meV)	t (ps)	τ_r (ps)
1	1468.0	1	+5.5	$\simeq +2$	85	115
2	1468.1	1.2	+0.2	$\leq \pm 0.5$	30	480
3	1468.2	1.3	0	$\simeq -2$	30	660

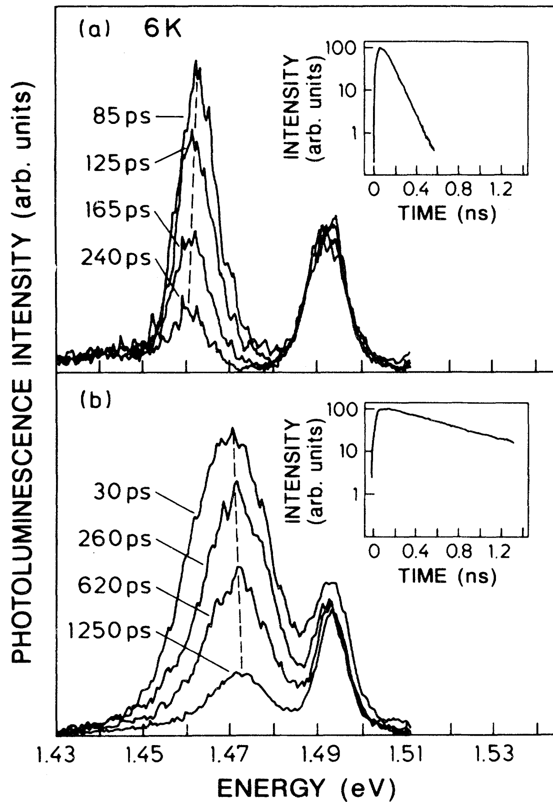

FIG. 6. Transient photoluminescence spectra taken at 6 K after pulsed excitation in resonance to the GaAs exciton (1.515 eV) for (a) sample No. 1 and (b) sample No. 3. The spectra are taken at different delay times after the arrival of the exciting pulse, as denoted in the figure. The dashed lines indicate the spectral diffusion of the emission in the course of time. In the insets, the time dependence of the spectrally integrated emission is shown on a semilogarithmic scale. Note the pronounced difference in the decay times of the two samples.

VI. DISCUSSION

Our experimental results fit a unique physical picture. The basic principle underlying the following considerations is the fact that the in-plane component of the central-cell potential of the isoelectronic InAs insertion creates an electronic state in the gap of the GaAs host material. This state leads to the localization of GaAs-type excitons perpendicular to the plane.[25] By restricting the lateral extent of the InAs insertion (samples No. 2 and 3), the translational motion of the excitons is additionally localized along the plane. The wave function of the localized exciton remains unaffected in either case, i.e., not its relative but its translational motion is localized. In other words, there is no confinement on the exciton, its wave function remains spherical, and its binding energy is that of the GaAs exciton. The lack of an effect on the *relative motion* is manifested by the coincidence of the optical transition energies of InAs planes and dots, i.e., the states have the same energy regardless of the lateral extent of the cluster. The precise evaluation of the localization energy as a function of the lateral size of the InAs insertion requires elaborate calculations that are beyond the scope of this paper. We note that the transition energy of InAs planes and dots observed in the optical spectra (1.468 eV) is almost identical to the one determined for InAs planes by self-consistent pseudopotential calculations (1.470 eV).[26] The effect of localization on the *translational motion* of the excitons is directly reflected by the observation of an exponential low-energy tail in the PL spectra of samples No. 2 and 3. Such an exponential density-of-states tail extending into the gap is expected whenever the wave function of the localized particle experiences a spatial distribution of electronic states.[27] Considering the actual Bohr radius of the GaAs exciton, it is obvious that the exciton experiences a set of quantum dots rather than an isolated one (see Fig. 3). The low-energy tails thus originate from the extension of the excitonic wave function over many of the localizing states. Here we will show that localization of the center-of-mass motion of excitons provides a unified physical explanation for the observed relaxation and recombination processes of the InAs planes and dots.

A. Recombination dynamics

Direct optical transitions via the interaction of excitons with photons are not possible in the presence of translational invariance, in which the crystal momentum is conserved. Excitons are then coherently coupled to the incident radiation field via their dipole moment, forming a quasistationary state of the crystal (the exciton polariton) whose energy is resonantly transferred between radiation and polarization fields.[28] Optical transitions in bulk crystals hence only occur via three-step processes, e.g., by the scattering of exciton-polaritons with acoustic phonons.[29] However, in the case of localization of the exciton, the translational invariance of the system is broken. Consequently, a density of states for direct optical transitions is introduced by the lack of wave-vector conservation. The excitonic transition is then entirely characterized by two experimentally accessible quantities, namely, the oscillator strength per unit cell $\tilde{f}$ and the radiative lifetime τ_r. These quantities are related to each other by

$$\tau_r = \frac{2\pi\epsilon_0 m_0 c^3}{\tilde{n} e^2 \omega^2 \tilde{f} N} , \tag{1}$$

with ω being the frequency of the transition, $\tilde{n}$ the refractive index accounting for the dielectric properties of the medium,[30] N the number of unit cells contributing to the emission process, and the other symbols having their usual meanings. The oscillator strength per unit cell uniquely determines the strength of the *absorption process.* On the other hand, the *emission process* in general occurs as the coherent superposition of the contributions of all unit cells over which the center-of-mass motion of the exciton persists (the so-called coherence area[31]). It is the product of the oscillator strength per unit cell and the number of unit cells which characterizes the strength of the spontaneous emission process.[31]

We first deduce the oscillator strength per unit cell from the transmission experiments shown in Fig. 5.

Within a two-dimensional model (energy loss per layer), the transmittance of sample with n absorbing layers is related to the dimensionless absorption probability p by

$$T=(1-p)^n . \quad (2)$$

The oscillator strength of the excitonic resonance is now properly defined per unit mesh and is extracted from the experimental spectrum (Fig. 5) by means of the relation[30]

$$\tilde{f}=\frac{4m_0\epsilon_0\tilde{n}ca_0^2}{e^2\pi\hbar}\int_0^\infty p(\hbar\omega)d(\hbar\omega) , \quad (3)$$

where a_0 is the in-plane lattice constant. The oscillator strength per unit mesh $\tilde{f}$ is determined to be 1×10^{-2} and 1.3×10^{-2} for samples No. 1 and 3, respectively. These numbers are computed neglecting the different In coverage of each plane. Thus, we actually still underestimate the oscillator strength for sample No. 3. This enhanced oscillator strength may originate from the modified density of states (DOS) when going from 2D to 0D systems. The difference in the oscillator strengths of samples No. 1 and 3, however, is opposite to the difference in radiative lifetimes. The temporal evolution of the spontaneous emission is indeed not only determined by the oscillator strength, as mentioned above, but predominantly by the coherence area.

Next we analyze the measured radiative lifetimes in order to gain quantitative insight into the nature of the coherence area. Both the InAs planes and dots are considered to be represented by sheets of an average lateral extent L and a height d. In either case, the height d is equal to one monolayer. The lateral extent L is equivalent to the spatial extent of areas with continuous In coverage. For InAs dots, the continuity of the In coverage is artificially restricted by the terrace size. For InAs planes, the In coverage is incomplete, leading to the formation of an InAs monolayer that is partially intersected by the GaAs matrix. The sheet area is thus directly determined by the structural configuration of the respective system, in that it is small for InAs dots and large for InAs planes. Thus, the center-of-mass motion of the exciton localized at the respective InAs insertion is (i) either truly 2D for $L>a_B$ or (ii) 0D for $L<a_B$, where a_B is the Bohr radius of the exciton which represents the space occupied by the relative motion of electron and hole. 2D-polariton effects are neglected by assuming that $L\ll\lambda$, where λ is the wavelength of the radiation field coupled to the exciton.

In case (i), the center-of-mass motion of the exciton extends over the whole area of the sheet. Then, all unit meshes within the InAs sheet area contribute to the emission process via the macroscopic polarization of the exciton. The number of unit cells N that enters into Eq. (1) can be identified with the number of unit meshes within the sheet area $[N=(L/a_0)^2]$. The exciton hence undergoes a superradiant decay[32-34] whose rate R is scaled by the characteristic dimension L:[35,36]

$$\begin{aligned} R &\simeq R_0|\langle x_e(z)|\chi_h(z)\rangle|^2\,|\phi_{\rm ex}^{\rm 2D}(0)|^2L^2 \\ &\simeq R_0|\langle \chi_e(z)|\chi_h(z)\rangle|^2\left[\frac{L}{a_B}\right]^2 , \end{aligned} \quad (4)$$

where R_0 is the dimensionless decay rate for interband transitions, $\langle\chi_e(z)|\chi_h(z)\rangle$ is the overlap integral of the electron and hole wave functions in the direction perpendicular to the InAs planes, and $\phi_{\rm ex}^{\rm 2D}$ is the wave function of the correlated relative motion along these planes.

In case (ii), the center-of-mass motion of the localized exciton is frozen out. As a consequence, the radiative decay rate is not enhanced by the factor (L/a_B) and no superradiant decay occurs, but atomiclike transitions are recovered. In terms of Eq. (1), the emission process is described by $N=(a_B/a_D)^2$. The transition rate is then given by the decay rate for interband transitions, which in turn is equivalent to the decay rate for atomic dipole-transitions:[37]

$$R_0=\frac{4\tilde{n}\omega^3}{3\hbar c^3}|\langle\mathbf{R}\rangle|^2 , \quad (5)$$

with $\langle\mathbf{R}\rangle$ being the electric dipole matrix element.[38]

Comparing the experimentally determined radiative lifetimes τ_r to those following from the expressions above $(\tau_r=R^{-1})$, we find that the lifetime of 660 ps measured for sample No. 3 is essentially equal to that for atomic dipole transitions, which amounts to about 600 ps. Thus, the InAs dots realized in this sample represent a genuine 0D system in the sense that the translational motion of the exciton is frozen out. The lifetime of 480 ps observed for sample No. 2 indicates the continuous transition in the intermediate range between the two limiting regimes (i) and (ii), as predicted theoretically.[39] On the other hand, the rapid decay of the luminescence observed in sample No. 1 reveals that the regime is entered where the center-of-mass motion freely extends over the sheet. The spatial extent of the sheet is determined by using Eq. (1) as well as Eq. (4) to about 30×30 nm^2, or equivalently 2800 unit meshes. The oscillator strength per sheet $(\tilde{f}N)$ is as large as 28 and thus indeed a "giant oscillator strength,"[40] in analogy to the case of excitons bound to shallow impurities.

B. Relaxation kinetics

Next, we discuss observations related to relaxation processes of excitons *to* and *within* the localized states. Note that the time-integrated luminescence efficiency L under resonant conditions is *independent* on the oscillator strength of the state but is only determined by the generation rate. Under nonresonant conditions (PL), the luminescence efficiency is predominantly determined by carrier capture by the emitting state. Under quasiresonant conditions (PLE close to the detection channel) the resonantly excited state has to relax to the specific recombination channel prior to radiative decay, which may limit the luminescence efficiency.[41] Experimentally, the PL efficiency of the InAs dots (sample No. 3) is two orders of magnitude *larger* than that of the InAs planes (sample No. 1), whereas the PLE efficiency is two orders of magnitude *smaller*. The enhanced PL efficiency of the InAs dots requires an enhanced trapping rate of photoexcited carriers generated in the continuum by the emitting state. The rise of the emission in the course of time monitors the relaxation of excitons *to* the emitting

state. For the InAs planes, the rise time directly reflects the relaxation of photoexcited carriers to the bottom of the band, which is delayed for perfect two-dimensional systems owing to the conservation of the exciton momentum along the layer.[42] In contrast, the in-plane symmetry is broken for zero-dimensional systems releasing excitons from wave-vector conservation, which means that they can decay radiatively as soon as they are trapped.

The drastically lower PLE efficiency of the InAs dots suggests that relaxation of the quasiresonantly excited state to the radiative channel is inhibited. In general, relaxation processes *within* the localized states manifest themselves (i) in the Stokes shift between the absorption- and emission-related transition and (ii) in the spectral diffusion of the emission, as observed in the transient luminescence spectra of sample No. 1 [Fig. 6(a)]. Indeed, the shift of the emission to *lower* energy is the time-resolved equivalent to the Stokes shift, i.e., it directly monitors the relaxation of the exciton towards the lowest-energy state. These states are presumably provided by atomic steps on top of the InAs sheets,[43,44] as suggested by the finding that neither the Stokes shift nor the spectral diffusion of the emission is observed in samples containing InAs submonolayer films of higher homogeneity (i.e., even closer agreement between experimental and theoretical diffraction patterns). Also, in sample No. 3 no Stokes shift is detected, but the emission of that sample shifts to *higher* energy in the course of time [Fig. 6(b)]. This spectral diffusion does not reflect a relaxation process, but indicates longer radiative lifetimes for high-energy states. Excitons apparently still populate high-energy states even 1 ns after the exciting pulse, which demonstrates that they are prohibited from relaxing toward the lowest-lying state. This inhibited relaxation process explains the small PLE efficiency and accounts also for the important high-energy broadening of the luminescence band (Fig. 4), which is observed neither in the transmission nor in the PLE spectra. The excitons decay radiatively *before* attaining the lowest-energy state, causing the high-energy emission as well as the lack of Stokes shift. The inhibited relaxation is probably related to the peculiar structural configuration of the system.[45] InAs dots are electronically isolated from each other by the high-energy barrier of the surrounding matrix. Excitons attached to the InAs dots thus do not have any degree of freedom in translational motion. Relaxation may then occur by tunneling rather than by phonon-assisted migration, i.e., spatial diffusion followed by trapping.[46] Of course, this intriguing observation deserves further studies for a quantitative understanding.

VII. CONCLUSION

To summarize, we have studied the structural and optical properties of InAs microclusters embedded in a single-crystal GaAs matrix. Fractional monolayers of InAs were deposited by molecular-beam epitaxy on vicinal (001) GaAs surfaces with an islandlike terrace configuration. The resulting structural configuration of the surface has been examined on an atomic scale by double-crystal x-ray diffractometry and transmission electron microscopy. These experiments have revealed that even in the presence of a high lattice strain of 7.16%, nucleation of In adatoms occurs by step propagation under appropriate growth conditions. The step-flow growth of InAs causes the formation of isolated InAs clusters on the step edges of the terraces. This peculiarity has allowed us the direct synthesis of InAs quantum dots in the subnanometer regime in a single-crystal matrix. The optical response of this intriguing system has been studied in detail. Our experiments have demonstrated that the optical response of excitons attached to the InAs insertions is uniquely controlled by the symmetry of the system, which in turn is given by the degree of freedom in translational motion. Lack of translational invariance releases the conservation of crystal momentum, determining the coupling of excitons to both photons and phonons, which in turn controls the radiative decay of the exciton as well as its relaxation to the radiating state. The incorporation of well-defined InAs microclusters in GaAs crystals now opens up an avenue to control of the translational symmetry of the crystal and thus to control of its optical response.

ACKNOWLEDGMENTS

We are indebted to A. Fischer for his continuous help with MBE growth and to G. C. La Rocca for many stimulating discussions. Thanks are due to M. Kelsch for HREM-sample preparation. This work was supported by the Bundesministerium für Forschung und Technologie of the Federal Republic of Germany.

*Present address: Centro Nazionale Ricerca e Sviluppo Materiali (CNRSM), I-70234 Messagne, Italy.

[1] L. E. Brus, J. Chem. Phys. **80**, 4403 (1984).

[2] S. Schmitt-Rink, D. A. B. Miller, and D. S. Chemla, Phys. Rev. B **35**, 8113 (1987).

[3] G. W. Bryant, Phys. Rev. B **37**, 8763 (1988).

[4] E. Hanamura, Phys. Rev. B **37**, 1273 (1988).

[5] Y. Kayanuma, Phys. Rev. B **38**, 9797 (1988).

[6] G. W. Bryant, Comments Condens. Mater. Phys. **14**, 277 (1989).

[7] A. D'Andrea and R. Del Sole, Solid State Commun. **74**, 1121 (1990).

[8] C. J. Sandroff, J. P. Harbison, R. Ramesh, M. J. Andrejco, M. S. Hedge, D. M. Hwang, C. C. Chang, and E. M. Vogel, Science **245**, 391 (1989).

[9] J. C. Luong and N. F. Borelli, in *Advances in Materials, Processing and Devices in III-V Compound Semiconductors*, edited by D. K. Sadana, L. E. Eastman, and R. Dupuis, MRS Symposia Proceedings No. 144 (Materials Research Society, Pittsburgh, 1989), p. 695.

[10] K. Kash, J. Lumin. **46**, 69 (1990).

[11] Y. Wang, N. Herron, W. Mahler, and A. Suna, J. Opt. Soc. Am. B **6**, 808 (1989).

[12] P. M. Petroff, A. C. Gossard, and W. Wiegmann, Appl. Phys.

Lett. **45**, 620 (1984).
[13]M. Tsuchiya, J. M. Gaines, R. H. Yan, R. J. Simes, P.O. Holtz, L. A. Coldren, and P. M. Petroff, Phys. Rev. Lett. **62**, 466 (1989).
[14]M. S. Miller, C. E. Pryor, H. Weman, L. A. Samoska, H. Kroemer, and P. M. Petroff, in *Proceedings of the 6th International Conference on Molecular Beam Epitaxy, San Diego, 1990* [J. Cryst. Growth **111**, 323 (1991)].
[15]S. A. Chalmers, H. Kroemer, and A. C. Gossard, Appl. Phys. Lett. **57**, 1751 (1990).
[16]J. H. Neave, P. J. Dobson, B. A. Joyce, and J. Zhang, Appl. Phys. Lett. **47**, 100 (1985).
[17]G. S. Bales and H. Zangwill, Phys. Rev. B **41**, 5500 (1990).
[18]H.-J. Gossmann, F. W. Sinden, and L. C. Feldman, J. Appl. Phys. **67**, 745 (1990).
[19]G. E. Crook, L. Däweritz, and K.Ploog, Phys. Rev. B **42**, 5126 (1990).
[20]S. A. Chalmers, A. C. Gossard, P. M. Petroff, J. M. Gaines, and H. Kroemer, J. Vac. Sci. Technol. B **7**, 1357 (1989).
[21]O. Brandt, L. Tapfer, R. Cingolani, K. Ploog, M. Hohenstein, and F. Phillipp, Phys. Rev. B **41**, 12 599 (1990).
[22]O. Brandt, K. Ploog, L. Tapfer, M. Hohenstein, and F. Phillipp (unpublished).
[23]D. A. Neumann, H. Zabel, and H. Morkoç, Appl. Phys. Lett. **43**, 59 (1983).
[24]O. Brandt, R. Cingolani, L. Tapfer, G. Scamarcio, and K. Ploog, Superlatt. Microstruct. **9**, 147 (1991).
[25]R. Cingolani, O. Brandt, L. Tapfer, G. Scamarcio, G. C. La Rocca, and K. Ploog, Phys. Rev. B **42**, 3209 (1990).
[26]K. Shiraishi and E. Yamaguchi, Phys. Rev. B **42**, 3064 (1990).
[27]B. I. Halperin and M. Lax, Phys. Rev. **148**, 722 (1966).
[28]J. J. Hopfield, Phys. Rev. **112**, 1555 (1958).
[29]W. J. Rappel, L. F. Feiner, and M. F. H. Schurmans, Phys. Rev. B **38**, 7874 (1988).
[30]D. L. Dexter, in *Solid State Physics,* edited by F. Seitz and D. Turnbull (Academic, New York, 1958), Vol. 6, p. 360.
[31]E.O. Göbel and K. Ploog, Prog. Quantum Electron. **14**, 289 (1991).
[32]R. H. Dicke, Phys. Rev. **93**, 99 (1954).
[33]Y. C. Lee and P. S. Lee, Phys. Rev. B **10**, 344 (1974); K. C. Liu, Y. C. Lee, and Y. Shan, *ibid.* **11**, 978 (1975).
[34]M. R. Philpott and P. G. Sherman, Phys. Rev. B **12**, 5381 (1975).
[35]E. Hanamura, Phys. Rev. B **38**, 1228 (1988).
[36]A. Nakamura, H. Yamada, and T. Tokizaki, Phys. Rev. B **40**, 8585 (1989).
[37]W. Heitler, *The Quantum Theory of Radiation,* 3rd. ed. (Clarendon, Oxford, 1954), p. 175.
[38]The amount of the electric dipole matrix element $\langle \mathbf{R} \rangle$ is to a very good approximation equal to the product of the elementary charge e, and the interatomic distance in the crystal lattice a_0. It can further be related to the familiar Kane's matrix element E_P ($\simeq 23$ eV) by $|\langle \mathbf{R} \rangle|^2 = e^2 E_p / 2\omega^2 m_0$. Both expressions yield $|\langle \mathbf{R} \rangle|^2 \simeq 10^{-56}$ C^2m^2.
[39]Y. Kayanuma and H. Momiji, Phys. Rev. B **41**, 10 261 (1990).
[40]E. I. Rashba, Fiz. Tekh. Poluprovdn. **8**, 1241 (1974) [Sov. Phys. Semicond. **8**, 807 (1975)].
[41]G. Bastard, *Wave Mechanics Applied to Semiconductor Heterostructures* (Les Editions de Physique, Les Ulis Cedex, 1988), p. 275.
[42]T. C. Damen, J. Shah, D. Y. Oberli, D. S. Chemla, J. E. Cunningham, and J. M. Kuo, Phys. Rev. B **42**, 7434 (1990).
[43]G. Bastard, C. Delalande, M. H. Meynadier, P. M. Frijlink, and M. Voos, Phys. Rev. B **29**, 7042 (1984).
[44]C. Delalande, M. H. Meynadier, and M. Voos, Phys. Rev. B **31**, 2497 (1985).
[45]J. A. Kash, Phys. Rev. B **29**, 7069 (1984).
[46]T. Takagahara, J. Lumin. **44**, 347 (1989).